Multiple scattering polarization – Application of Chandrasekhar's formalisms to the atmosphere of brown dwarfs and extrasolar planets

SUJAN SENGUPTA[1,*] and MARK S MARLEY[2]

[1]Indian Institute of Astrophysics, Koramangala 2nd Block, Bangalore 560 034, India
[2]NASA Ames Research Center, Moffett Field, CA 94035, USA
*Corresponding author. E-mail: sujan@iiap.res.in

Abstract. Chandrasekhar's formalisms for the transfer of polarized radiation are used to explain the observed dust scattering polarization of brown dwarfs in the optical band. Model polarization profiles for hot and young directly imaged extrasolar planets are presented with specific prediction of the degree of polarization in the infrared. The model invokes Chandrasekhar's formalism for the rotation-induced oblateness of the objects that gives rise to the necessary asymmetry for yielding net non-zero disk integrated linear polarization. The observed optical polarization constrains the surface gravity and could be a tool to estimate the mass of extrasolar planets.

Keywords. Scattering; polarization; atmosphere; brown dwarfs; extrasolar planets.

PACS Nos 97.20.Vs; 97.82.-j; 95.30.Jx; 97.10.Ex

1. Introduction

When a beam of radiation traverses through a medium, it interacts with the material of the medium and carries the information of the medium to a detector. The history of this radiation is described by the radiative transfer equations which were first formulated by Chandrasekhar [1] for the application to astrophysics. The flux or the spectrum obtained from a stellar object is modelled by solving simultaneously and self-consistently the radiative transfer equations, the hydrostatic equilibrium equation, the radiative equilibrium equation, the statistical equilibrium equation and the charge conservation equation. For a substellar mass object such as a brown dwarf or a gaseous planet, the chemical equilibrium equation is also included in the set of equations. By fitting the synthetic spectrum with the observed spectrum, two most important physical parameters – the effective temperature and the surface gravity of the stellar and substellar objects are determined. This also provides atomic and molecular abundances of the object. Chandrasekhar [1] also generalized the scalar radiative transfer equations into vector radiative transfer equations to incorporate scattering polarization of the radiation. He deduced the scattering phase functions that provide the distribution of photons before and after Thomson scattering or Rayleigh scattering.

In §2, the radiative transfer equation both in its scalar and vector forms and the scattering phase functions for different types of scattering are briefly discussed. A brief introduction about brown dwarfs and exoplanets is provided in §3. The general atmospheric properties of substellar mass objects are provided in §4. The theoretical model that is used to analyse the observed linear polarization of dusty and warm brown dwarfs is described in §5. The use of polarimetry in constraining the mass of brown dwarfs and exoplanets as well as for determining the climate of these substellar mass objects by solving the polarization radiative transfer equations are discussed in §6. Finally, specific conclusions are presented in §7.

2. Chandrasekhar's formalisms of radiative transfer

2.1 *The transfer equations*

From the energy conservation, the most general time-independent radiative transfer equation can be written as [1]

$$\frac{\mathrm{d}I_v}{\mathrm{d}s} = -\kappa_v \rho I_v + j_v \rho, \tag{1}$$

where I_v is the specific intensity or simply the intensity of radiation which depends on the frequency and direction so that the 'Chandrasekhar flux' can be written as

$$\pi F_v = \int I_v \cos\theta \, \mathrm{d}\omega, \tag{2}$$

where θ is the angle at which the energy flow across an element area of $\mathrm{d}\sigma$ is inclined to its outward normal and confined to an element of solid angle $\mathrm{d}\omega$. κ_v and j_v are the mass absorption and emission coefficients for radiation of frequency v, ρ is the density of the material through which the radiation passes and $\mathrm{d}s$ is the thickness of the medium in the direction of propagation of radiation.

If the medium in which the transfer of radiation is considered has spherical symmetry and if there is no incident radiation from the outside, then eq. (1) can be written as

$$\mu \frac{\partial I(v, \mu, r)}{\partial r} + \frac{1 - \mu^2}{r} \frac{\partial I(v, \mu, r)}{\partial \mu} = j(v, mu, r) - \chi(v, \mu, r) I(v, \mu, r), \tag{3}$$

where $\mu = \cos\theta$ and r is the radius vector.

If the medium is stratified in parallel planes in which all the physical properties are invariant over a plane, then eq. (1) can be written as

$$\mu \frac{\mathrm{d}I(v, \mu, \tau)}{\mathrm{d}\tau} = I(v, \mu, \tau) - \frac{\omega}{2} \int_{-1}^{+1} p(\mu, \mu') I(v, \mu, \tau) \mathrm{d}\mu', \tag{4}$$

where $\mathrm{d}\tau = \chi \, \mathrm{d}z$ (or $\chi \, \mathrm{d}r$ in spherical geometry) and z is the axis of symmetry. τ is called the optical depth of the medium which is the inverse of the distance traversed by a photon before it gets completely removed from the radiation field. Note that χ is known as extinction coefficient which is the sum of the true absorption and scattering coefficients. Chandrasekhar used the notation κ to represent the extinction coefficient. $p(\mu, \mu')$ is

called the scattering phase function which provides the angular distribution of the photon before and after scattering and ω is called the albedo for single scattering which provides the fraction of radiation that is scattered. To describe the geometry of the atmosphere of normal stars like the Sun and planets whose radius is comparatively small, plane-parallel approximation is sufficient.

For planetary atmosphere where radiation from the parent star is incident on the upper boundary of the atmosphere, the radiative transfer equation can be written as

$$\mu \frac{dI(\nu, \mu, \tau)}{d\tau} = I(\nu, \mu, \tau) - \frac{\omega}{2} \int_{-1}^{+1} p(\mu, \mu') I(\nu, \mu, \tau) d\mu'$$
$$- \frac{\omega}{4} F_\nu e^{-\tau/\mu_0} p(\mu, \mu_0), \tag{5}$$

where F_ν is the incident flux from the star and μ_0 is the direction at which it is incident on the surface of the planet.

The above equations formulated by Chandrasekhar provide the scalar radiation field. Chandrasekhar [1], for the first time, introduced the Stokes parameters in the equation of radiative transfer with a slight modification of Stoke's representation and formulated the vector radiative transfer equations that describe the scattering polarization state of the radiation. In spherical geometry the vector radiative transfer equations can be written as

$$\mu \frac{\partial \mathbf{I}(\nu, \mu, r)}{\partial r} + \frac{1 - \mu^2}{r} \frac{\partial \mathbf{I}(\nu, \mu, r)}{\partial \mu} = j(\nu, \mu, r) - \chi(\nu, \mu, r) \mathbf{I}(\nu, \mu, r), \tag{6}$$

where $\mathbf{I} = [I, Q, U, V]^{-1}$, I, Q, U and V being the Stokes parameters representing the total intensity I and the polarized intensities Q, U and V. For linear polarization, $V = 0$.

On the other hand, in a plane-parallel atmosphere with no incident radiation, the plane of polarization is along the meridian plane which makes $U = V = 0$. Hence the corresponding equations can be write as

$$\mu \frac{d\mathbf{I}(\nu, \mu, \tau)}{d\tau} = \mathbf{I}(\nu, \mu, \tau) - \frac{\omega}{2} \int_{-1}^{+1} \mathbf{P}(\mu, \mu') \mathbf{I}(\nu, \mu, \tau) d\mu', \tag{7}$$

where $\mathbf{I} = [I, Q]^{-1}$ and $\mathbf{P}(\mu, \mu')$ is the phase matrix given in the next section. The degree of polarization in general is given as

$$p = \frac{\sqrt{Q^2 + U^2 + V^2}}{I}. \tag{8}$$

2.2 *The scattering phase matrix*

The theory of scattering depends on the size and properties of the scatterer. Scattering by non-relativistic electrons is described by Thomson's law and scattering by atoms and molecules is described by Rayleigh's law. While Thomson scattering cross-section is independent of the wavelength of the photon, the cross-section for Rayleigh scattering depends on the wavelength as well as the optical properties of the scatterer. However, Chandrasekhar found that the angular distribution of the photon remains the same for both Thomson and Rayleigh scatterings. For Thomson and Rayleigh scatterings, Chandrasekhar derived the most general phase matrix that is related to all the four Stokes intensities and

depends on both the polar and azimuthal angles. The phase matrix for a plane-parallel medium in which $U = V = 0$ and the radiation field is azimuth independent because of the axial symmetry can be written as

$$\mathbf{P}(\mu, \mu') = \frac{3}{4} \begin{pmatrix} 2\left(1 - \mu^2\right)\left(1 - \mu'^2\right) + \mu^2\mu'^2 & \mu^2 \\ \mu'^2 & 1 \end{pmatrix}. \tag{9}$$

The scattering by dust is described by Mie theory and the cross-section depends on the size of the scatterer. The phase function for Mie scattering has to be derived numerically. However, it is well reproduced by Henyey–Greenstein empirical function

$$h(\Theta, g) = \frac{1}{2} \frac{1 - g^2}{\left(1 + g^2 - 2g\cos\Theta\right)^{3/2}}, \tag{10}$$

where g is the scattering asymmetric parameter and Θ is the angle between the direction of photon before and after scattering.

For polarization by dust scattering in a plane-parallel medium, the convolution of Chandrasekhar's phase matrix for Rayleigh scattering and Henyey–Greenstein phase function is adopted so that for scattering by sufficiently small particle, Mie scattering phase matrix reduces to Rayleigh scattering phase matrix. We call it Chandrasekhar–Henyey–Greenstein phase matrix.

To calculate scattering polarization of the atmosphere of a stellar or planetary atmosphere, the radiative transfer equation in its vector form has to be solved along with appropriate boundary conditions. The optical depth and the atmospheric temperature as a function of geometrical depth are provided as input parameters. However, to calculate the emergent flux and the polarization profile self-consistently and correctly, the radiative transfer equations are solved simultaneously with the hydrostatic equilibrium equation, radiative equilibrium equation, statistical equilibrium equation and the charge conservation equation. For a cool atmosphere such as that of a brown dwarf or planet, chemical equilibrium equation also is to be solved as various molecules are formed at different depths.

3. Substellar mass objects

We apply, for the first time [2–4], Chandrasekhar's formalism to estimate scattering polarization of the atmosphere of substellar mass objects. As the atmosphere of these objects is sufficiently cool, condensation of various molecular species takes place at the visible atmosphere and scattering by condensates yields detectable amount of polarization.

Substellar mass objects (SMO) are mainly of two types – brown dwarfs and extrasolar planets.

3.1 *Brown dwarfs*

Brown dwarfs are objects less massive than the lightest stars but heavier than the heaviest planets. They serve as the link between stars and planets. Brown dwarfs are understood to be formed like a star – through the gravitational collapse of interstellar cloud. They have sufficient mass (typically greater than $0.011 M_\odot$) to ignite deuterium in their core but they fail to ignite lithium due to the lack of enough mass (less than $0.084 M_\odot$). Hence they could

not sustain hydrogen fusion at their core. Therefore, these objects do not have an internal source of energy and the thermal radiation from brown dwarfs arises from the release of gravitational potential energy during their formation and governed by the interaction with the atmospheric material [5].

The distinct features of the spectra of brown dwarfs, e.g., gradual disappearance of VO, TiO etc. and appearance of hydrides such as CaH, CrH, FeH etc., compel astronomers to introduce two more classes in the stellar spectral classification [6]. The relatively warmer objects whose effective temperature ranges between 2400 and 1300 K are considered to be L dwarfs. The L dwarfs which show clear signature of primordial Li in their spectra are brown dwarfs. The cooler objects that show methane in their spectra are known as T dwarfs or methane dwarfs and all T dwarfs are brown dwarfs. The effective temperature of T dwarfs ranges between 600 and 1300 K.

The surface gravity of brown dwarfs are poorly constrained and ranges from 3000 to 300 m s^{-2}. The radii of brown dwarfs are almost independent of their age or mass and typically the same as the radius of Jupiter.

3.2 *Extrasolar planets*

Since the discovery of the first confirmed extrasolar planet around the star 51 Pegasi in 1995, more than 500 planets around stars of various spectral types have been discovered by different methods. The physical properties of these planets have revolutionized our concept on planets and planetary systems. A large number of exoplanets are discovered mainly by radial velocity method, transit method, gravitational microlensing method, timing method and imaging method. Most of these planets are gas giants and orbiting very close to their parent stars and so they are strongly irradiated. The limitations of various existing detection methods are that they can find out planets that are a few times more massive than Neptune and very close to their parent star. However, recently a few young and hot planets are discovered, resolved from their parent star and imaged. These planets are far away from their stars and therefore not irradiated. Since the atmospheric temperature of such planets are very similar to that of the warm brown dwarfs, they should have similar atmospheric properties such as the presence of dust clouds in the visible region.

4. Dusty atmosphere of substellar objects

4.1 *Brown dwarfs*

Brown dwarfs belong to the class of ultracool dwarfs whose atmospheric low temperature and high pressure initiate the formation of molecular clouds composed of refractory compounds. Detailed investigations on the complex atmosphere and synthetic spectra of brown dwarfs imply that the condensates or dust particles form at a certain atmospheric height where they act as efficient element sink leaving behind a depleted gas phase. This scenario is confirmed by the gradual disappearance of TiO, VO, etc. in the spectra from M to L dwarfs. As the objects cool down, the dust settles down gravitationally beyond the visible atmosphere taking condensed matter with it. Hence dust cloud is not expected in the visible atmosphere of the cooler T dwarfs [7].

Usually, the observed spectra and photometry of brown dwarfs are used to testify the synthetic spectra that incorporate our present understanding of atmospheric physics, chemistry, dynamics and cloud processes. In addition to this, the parameter space is narrowed down by the evolution models [8,9]. However, one of the most important parameters, the surface gravity of these objects, is still poorly constrained. Theoretical reproduction of the observed spectra as well as the evolution model allow the surface gravity to vary from 300 to 3000 m s^{-2}. Therefore, a completely different observational information that arises due to the atmospheric processes is essential in addition to the spectra and image of the objects. Image polarimetry serves this requirement.

Following the theoretical prediction [10], polarimetric observation covering almost the entire range of spectral type L0-L8 lead to the detection of linear polarization in the optical bands from a good number of L dwarfs [11–13]. The observed polarization could arise either by scattering or by the presence of magnetic field – either from Zeeman splitting of atomic or molecular lines or synchrotron emission. Individual and simultaneous radio, X-ray, ultraviolet and Hα observations imply a lack of even moderate magnetic activity in mature field L dwarfs [14]. If the radio emission that peaks at 8.3 GHz, as detected from a few L dwarfs, is coronal, magnetic fields in the range 100–1000 G should be present. This implies that the resulting synchrotron processes will not lead to significant linear polarization in the optical. By comparing the net linear polarization as small as a few times of 0.01% detected from a sample of Ap stars [15] having about 1 kG surface dipolar field, Menard *et al* [11] argued that the observed optical linear polarization of ultracool dwarfs could not be explained by Zeeman splitting of atoms or molecules. At the same time, polarization is reported neither from M dwarfs nor from the cooler T dwarfs that have no dust cloud in the visible atmosphere although M dwarfs should have stronger magnetic field [16].

On the other hand, single scattering model in a rotation-induced oblate atmosphere could explain the observed polarization [17,18]. Therefore, dust scattering polarization is the only plausible physical process that can account for the observed polarization of L dwarfs. However, single scattering model does not incorporate the full physical environment and often overestimate the amount of polarization. Therefore, detailed multiscattering modelling by solving Chandrasekhar's vector radiative transfer equation is essential to analyse the polarimetric observations.

4.2 *Extrasolar planets*

Formation of silicate clouds in the visible atmosphere of hot exoplanets and water clouds in cooler ones are favourable due to relatively lower atmospheric pressure. Phase-dependent linear polarization of irradiated gaseous exoplanets has been predicted [19–22] by considering the scattering of silicate condensates in the atmosphere. However, as these planets are too close to be resolved from their parent stars, the unpolarized continuum radiation from the star makes the net polarization too small to be detected. Very recently, a few young and hot planets such as the four planets around HR 8799, one around 2MASS 1207 and another around Beta Pictoris were directly imaged. The atmospheric properties of these planets should be very similar to that of L dwarfs – the warmer brown dwarfs. Further, irradiation from the star is too weak to influence the atmosphere of such planets.

Similar to the ambiguous situation of surface gravity for brown dwarfs, the surface gravity of directly imaged extrasolar planets and hence their mass cannot be determined

confidently because radial velocity measurement of these planets orbiting several AU away from their parent stars is not possible. The situation becomes complicated because the radii of exoplanets strongly depend on their age and mass and hence unlike brown dwarfs, the surface gravity of extrasolar planets cannot provide their mass directly. Due to the lack of proper understanding of the initial condition, the surface gravity cannot be determined accurately from the luminosity–age relationship. Hence disk integrated scattering polarization which is sensitive to the shape of the disk can be used as a tool to estimate the mass of exoplanets.

5. Theoretical model

5.1 *Atmospheric model*

To reproduce the observed polarization of the L dwarfs and to predict the amount of polarization of extrasolar planets that could be directly imaged, we employ a grid of one-dimensional, plane-parallel, hydrostatic, non-gray, radiative–convective equilibrium atmosphere model that includes about 2200 gas species, about 1700 solids and liquids for compounds of 83 naturally occurring elements and five major condensates as opacity sources [23,24]. A log-normal particle size distribution that intends to capture the doubled-peaked size distribution in terrestrial rain clouds is adopted. The present model uniquely predicts the mean particle size and particle number density along the atmospheric depth which plays a crucial role in determining the scattering polarization. In this model, small particles with mean radius less than 0.01 μm populate the upper cloud region. The particle sizes increase inwards and reach a certain maximum value. This is a common feature in almost all existing atmospheric models of substellar objects [7].

The atmospheric code derives the gas and dust opacity, the temperature–pressure profile and the dust scattering asymmetry function averaged over each atmospheric pressure level by solving Chandrasekhar's scalar radiative transfer equations self-consistently along with the various equilibrium equations. These quantities are then used as inputs in a multiple scattering polarization code that solves the radiative transfer equations in vector form as given by Chandrasekhar to calculate the linear polarization in a locally plane-parallel medium. Finally, the polarization is integrated over the rotation-induced oblate disk of the object using a spherical harmonic expansion method [2].

5.2 *Shape of the object: Darwin–Radau–Chandrasekhar relationship*

The observation of non-zero polarization from unresolved objects indicates either the non-sphericity of spatially homogeneous atmosphere or spherical but inhomogeneous atmosphere or both. The non-sphericity may result from several causes. Rotation of a stellar object results in an oblate ellipsoid, as is evident in the outer solar planets. Apart from rotational effects, tidal interaction with the companion in a binary system also imposes an ellipsoidal shape extending towards the companion. Spectroscopic studies [25] indicate rapid rotation of brown dwarfs along their axis and hence the shape of the object is expected to be non-spherical giving rise to the necessary asymmetry that yields net non-zero disk-integrated polarization.

The relationship for the oblateness f of a stable polytropic gas configuration under hydrostatic equilibrium is derived by Chandrasekhar [26] and can be written as

$$f = \frac{2}{3} C \frac{\Omega^2 R_e^3}{GM}, \tag{11}$$

where M is the total mass, R_e is the equatorial radius, Ω is the angular velocity of the object and C is a constant whose value depends on the polytropic index. For the polytropic index $n = 0$, the density is uniform and $C = 1.875$. This configuration is known as the Maclaurin spheroid. For a polytropic index of $n = 1$, $C = 1.1399$, which is appropriate for Jupiter. For non-relativistic completely degenerate gas, $n = 1.5$ and $C = 0.9669$.

On the other hand, Darwin and Radau also derived independently an expression for the rotation-induced oblateness which is given by [27]

$$f = \frac{\Omega^2 R_e^3}{GM} \left[\frac{5}{2} \left(1 - \frac{3}{2} K \right)^2 + \frac{2}{5} \right]^{-1}. \tag{12}$$

In eq. (12), $K = I/MR_e^2 \leq 2/3$ where I is the moment of inertia of the spherical configuration.

Although the expressions above are independently derived by Darwin, Radau and Chandrasekhar, they gave the same value of oblateness for a given mass, radius and rotational velocity. In fact, equating the above two expressions, and putting the value of the moment of inertia for any polytropic index n, one can derive exactly the same numerical
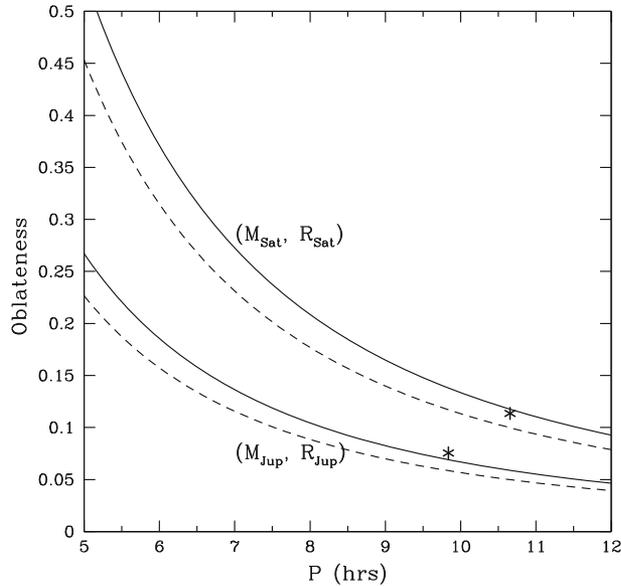

Figure 1. Rotation-induced oblateness as a function of rotation period for mass and radius of Jupiter and Saturn. The solid lines represent the oblateness for the polytropic index $n = 1$ and the dashed lines represent that for $n = 1.5$. The stars indicate the observationally inferred oblateness of Jupiter and Saturn at 1 bar pressure.

values of C that Chandrasekhar calculated. As shown in figure 1, Darwin–Radau–Chandrasekhar relationship provides the oblateness of Jupiter and Saturn very near to their observed values if the matter distribution is assumed to be polytropic with index $n = 1$.

6. Results and discussion

The polarization models constructed using the above methods are compared to the observed polarization of L dwarfs of different spectral types and hence different effective temperature as derived from the synthetic spectra.

Out of the 15 L dwarfs [3] whose observed I band polarization is considered, the projected rotational velocity $V \sin(i)$ for seven of them are known from high resolution spectroscopy. 2MASS J1412 (L0.5) has the minimum $V \sin(i)$ of 19 km s^{-1} [28] and 2MASSW J1807 (L1.5) has the maximum $V \sin(i)$ of 76 km s^{-1} [28]. However, the projection angle i is not known for any of the cases. If we assume $i = 90°$ then $V \sin(i) = 48$ km s^{-1} gives the rotational velocity $V = 48$ km s^{-1} and for $g = 1000$ m s^{-2} Darwin–Radau–Chandrasekhar formula for a polytrope of index $n = 1$ yields an oblateness of 0.024 for a typical brown dwarf radius of $1R_{\text{Jup}}$. But this is too small to produce the
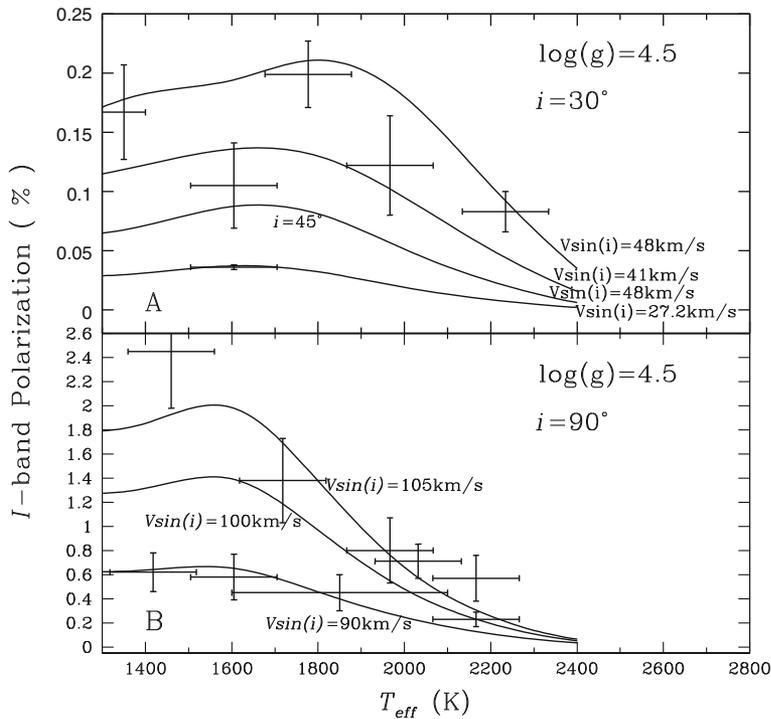

Figure 2. Best fit models of the observed I-band linear polarization of brown dwarfs. The vertical error bars are observational errors and the horizontal error bars are the spread of effective temperature for a particular spectral type. In the upper panel $i = 30°$ for all the cases except the one marked otherwise. In the lower panel $i = 90°$.

observed I-band polarization $p = 0.167 \pm 0.04$ of DENIS-P J0255, an object of spectral type L8 (corresponding $T_{\text{eff}} = 1500 \pm 100$ K) with known projected rotational velocity 40.8 ± 8 km s^{-1} [25]. On the other hand, if we assume that the projection angle $i = 30°$ then $V \sin(i) = 48$ km s^{-1} gives the rotational velocity $V = 96$ km s^{-1} which yields an oblateness $f = 0.097$, still insufficient to produce the observed I-band polarization of the object. A further decrease in the value of i although increases the value of V and hence the oblateness, reduces polarization substantially. Therefore, the only way to achieve the required degree of polarization is to reduce the surface gravity and we obtain a good fit with the observational data by setting the surface gravity at 300 m s^{-2}. As shown in figure 2, five of the observational data points can fit well with just two values of $V \sin(i)$ equal to 48 km s^{-1} and 41 km s^{-1} by setting $i = 30°$ and $g = 300$ m s^{-2}. Figure 2 also shows that the observed polarization of DENIS-P J0255 cannot be achieved from its observed projected rotational velocity if $i = 45°$. The observed [13] I-band polarization of 2MASSW J1507 fits well by using the observed projected rotational velocity $V \sin(i) = 27.2$ km s^{-1} [29] in a model with $g = 300$ m s^{-2} and $i = 30°$. The effective temperature of this object of
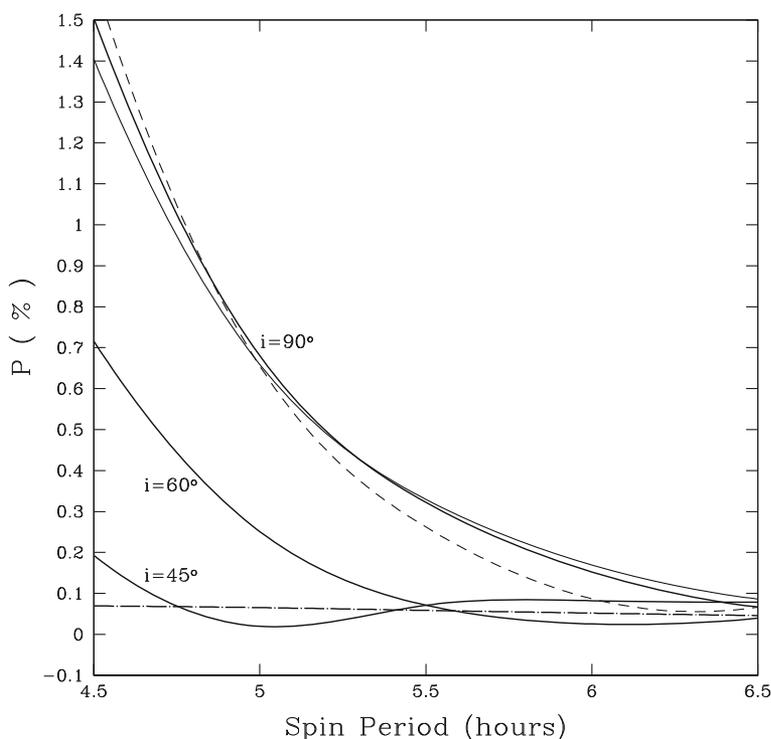

Figure 3. Model prediction of J band linear polarization from directly imaged, hot and young extrasolar planets. The three thick solid lines represent models with $T_{\text{eff}} = 1000$ K and $g = 30$ m s^{-2} but with different viewing angles i. The thin solid line represents model with $T_{\text{eff}} = 1200$ K and $g = 30$ m s^{-2}. The dashed line represents model with $T_{\text{eff}} = 800$ K and $g = 30$ m s^{-2}. The dashed–dot line represents model with $T_{\text{eff}} = 1200$ K and $i = 90°$ but $g = 100$ m s^{-2}.

spectral type L5 is 1700 ± 100 K. The linear polarization of a few L dwarfs, detected in I- and R-bands by Zapatero Osorio *et al* [12] are even higher and possibly need a lower surface gravity to account for. We find that the observed polarization of these objects can be explained if their projected rotational velocity is as high as 90–105 km s^{-1} with the inclination angle $i = 90°$ and $g = 300$ m s^{-2}.

For the directly imaged exoplanets that are resolved, our prediction for scattering linear polarization in J-band is presented in figure 3 for a range of effective temperatures between 800 and 1200 K and surface gravity 30 m s^{-2}. The radius of the object is calculated from their age corresponding to their effective temperature. The polarization may not be detectable for any rotational velocity if the surface gravities of the planets are higher than about 50 m s^{-2}. Hence polarimteric observation of such exoplanets could help in constraining the surface gravity [4].

We emphasize that the atmosphere model employed here determines the dust distribution and size quite naturally and the model is fundamentally the same as all the other atmosphere models of brown dwarfs and hot exoplanets. Therefore, any ad-hoc inclusion of dust bands or thin haze consisting of arbitrary particle size may increase the polarization but would be inconsistent with the observed spectra of L dwarfs and photometric properties of exoplanets. Atmospheric activity may at most give rise to variable polarization but it cannot increase the degree of polarization sufficiently. Photometric variability is detected from a few brown dwarfs [30]. However, no co-relation is found between variability and polarization. No polarization is detected of a few variable L dwarfs. On the other hand, a few polarized L dwarfs show no photometric variability. Hence, inhomogeneity, if any, may not yield polarization comparable to the amount of polarization that arises from a rotationally oblate object.

7. Conclusion

Our theoretical prediction that atmospheric dust scattering would give rise to detectable amount of linear polarization in the optical bands of brown dwarfs has been confirmed by the detection of polarization of a large number of warmer brown dwarfs or L dwarfs. We use Chandrasekhar's formalism to model the observed polarization by solving the multiple scattering radiative transfer equations in its vector form by considering spatially uniform dust distribution. The polarization calculated in a locally plane-parallel atmosphere is integrated over the rotation-induced oblate disk of the object. The rotation-induced oblateness is derived from the observationally inferred projected rotational velocity and by using Darwin–Radau–Chandrasekhar relationship. We find that the detected polarization severely constrains the surface gravity of brown dwarfs. Polarization also serves as an important indicator for the presence of dust cloud and can probe the transition from dusty L dwarfs to cloud-free T dwarfs. We also model the dust scattering polarization that may arise from the atmosphere of directly imaged hot and young exoplanets. Future detection of polarization of exoplanets may be used to constrain the surface gravity of such planets.

References

[1] S Chandrasekhar, *Radiative Transfer* (Dover, New York, 1960)
[2] S Sengupta and M S Marley, *Astrophys. J.* **707**, 716 (2009)

[3] S Sengupta and M S Marley, *Astrophys. J. Lett.* **722**, L142 (2010)
[4] M S Marley and S Sengupta, *Bull. Am. Astron. Soc.* **42**, 1063 (2010)
[5] A Burrows, W B Hubbard, J I Lunine and J Liebert, *Rev. Mod. Phys.* **73**, 719 (2001)
[6] J D Kirkpatrick, *Annu. Rev. Astron. Astrophys.* **43**, 195 (2005)
[7] Ch Helling *et al*, *Mon. Not. R. Astron. Soc.* **391**, 1854 (2008)
[8] D Saumon and M S Marley, *Astrophys. J.* **689**, 1327 (2008)
[9] I Baraffe *et al*, *Astron. Astrophys.* **382**, 563 (2002)
[10] S Sengupta and V Krishan, *Astrophys. J. Lett.* **561**, L123 (2001)
[11] F Menard, X Delfosse and J L Monin, *Astron. Astrophys.* **396**, L35 (2002)
[12] M R Zapatero Osorio, J A Caballero and V J S Bejar, *Astrophys. J.* **621**, 445 (2005)
[13] R Tata *et al*, *Astron. Astrophys.* **508**, 1423 (2009)
[14] E Berger *et al*, *Astrophys. J.* **709**, 332 (2010)
[15] J L Leroy, *Astron. Astrophys. Suppl.* **114**, 79 (1995)
[16] S Mohanty *et al*, *Astrophys. J.* **571**, 469 (2002)
[17] S Sengupta, *Astrophys. J. Lett.* **585**, L155 (2003)
[18] S Sengupta and S Kwok, *Astrophys. J.* **625**, 996 (2005)
[19] S Sengupta and M Maiti, *Astrophys. J.* **639**, 1147 (2006)
[20] S Sengupta, *Astrophys. J. Lett.* **683**, L195 (2008)
[21] S Seager, B A Whitney and D Sasselov, *Astrophys. J.* **540**, 504 (2000)
[22] D M Stam *et al*, *Astron. Astrophys.* **452**, 669 (2006)
[23] A Ackerman and M S Marley, *Astrophys. J.* **556**, 872 (2001)
[24] M S Marley *et al*, *Astrophys. J.* **568**, 335 (2002)
[25] S Mohanty and G Basri, *Astrophys. J.* **583**, 451 (2003)
[26] S Chandrasekhar, *Mon. Not. R. Astron. Soc.* **93**, 539 (1933)
[27] J W Barnes and J J Fortney, *Astrophys. J.* **588**, 545 (2003)
[28] A Reiners and G Basri, *Astrophys. J.* **684**, 1390 (2008)
[29] C A L Bailer-Jones, *Astron. Astrophys.* **419**, 703 (2004)
[30] M Maiti, S Sengupta, P S Parihar and G C Anupama, *Astrophys. J. Lett.* **619**, L183 (2003)